Rheology of miscible blends of poly(methyl methacrylate) with poly(styrene-*co*-acrylonitrile) and with poly(vinylidene fluoride)

Heng-Huey Yang and Chang Dae Han*
Department of Chemical Engineering, Polytechnic University, Brooklyn, NY 11201, USA

and Jin Kon Kim
Research and Development Center, Petrochemicals and Polymers, Lucky Ltd, Science Town, Daejeon 305-343, Korea
(Received 9 December 1992; revised 8 June 1993)

The rheological behaviour of miscible blends of poly(methyl methacrylate) (PMMA) with poly(styrene-*co*-acrylonitrile) (PSAN) and with poly(vinylidene fluoride) (PVDF), in the molten state, was investigated. For this study, both steady and oscillatory shear flow measurements were made for PMMA/PVDF and PMMA/PSAN blends, which were prepared by melt blending in a twin-screw compounding machine. The following observations were made from the experimental results obtained: (1) plots of the logarithm of the zero-shear viscosity ($\log \eta_{ob}$) *versus* blend composition show *positive* deviations from linearity for the PMMA/PSAN blend system, but *negative* deviations from linearity for the corresponding PMMA/PVDF system, under isothermal conditions; (2) plots of $\log \eta_{ob}$ *versus* blend composition for the PMMA/PVDF blend system show minimum values at certain blend compositions as the viscosity ratio of the constituent components becomes smaller than a certain critical value and; (3) logarithmic plots of the dynamic storage modulus (G') *versus* the dynamic loss modulus (G'') for all of the blend compositions lie between those obtained for the constituent components in both of the PMMA/PSAN and PMMA/PVDF blend systems. The experimental results are interpreted by using a molecular viscoelasticity theory recently developed by Han and Kim.

(Keywords: rheology; PMMA/PVDF blends; PMMA/PSAN blends)

INTRODUCTION

Over the past two decades a number of polymer pairs have been found to be miscible. As there are far too many to cite here, interested readers are therefore referred to the relevant literature[1,2]. During the past decade measurements of the rheological properties of these miscible polymer blends have been reported[3–19]. Recently, Han and Kim[20,21] developed a molecular viscoelasticity theory, which enables one to predict the linear viscoelastic properties of miscible polymer blends, and showed that plots of the logarithm of zero-shear viscosity *versus* blend composition under isothermal conditions exhibit *negative* deviations from linearity for binary blends having large, negative values of the interaction parameter χ, and *positive* deviations from linearity for blends having extremely small, positive values of χ.

In this paper we shall report on our recent experimental study of both the steady and oscillatory shear flow properties of miscible blends of poly(methyl methacrylate) (PMMA) with both poly(styrene-*co*-acrylonitrile) (PSAN) and poly(vinylidene fluoride) (PVDF), and then interpret the experimental results using the molecular theory of Han and Kim[20,21]. Earlier, Wu[9,10] had reported experimental results of only the oscillatory shear flow properties of PMMA/PSAN and PMMA/PVDF blend systems. It should be mentioned here that various other research groups have also investigated the miscibility of PMMA/PSAN[22–27] and PMMA/PVDF blends[28–34].

*To whom correspondence should be addressed. Present address: Department of Polymer Engineering and Institute of Polymer Engineering, The University of Akron, Akron, OH 44325, USA

EXPERIMENTAL

Materials

The materials used in this study were commercial grades of PMMA, PSAN and PVDF. *Table 1* gives a summary of the molecular weights of the polymers that were employed. The molecular weight and molecular weight distribution of PMMA were determined via gel permeation chromatography (g.p.c.) using tetrahydrofuran as the solvent, and with a monodisperse PMMA, obtained from the American Standards Company, being used as a standard. The amount of acrylonitrile (AN) in PSAN, which was determined by elemental analysis, was found to be 25.3 wt%. The molecular weight of PSAN was also determined by g.p.c., using various monodisperse polystyrenes as standards. Information concerning the molecular weight of PVDF was supplied by

0032-3861/94/07/1503-09

Table 1 Molecular characteristics of the polymers investigated

Polymer/copolymer	Abbreviation	M_w ($\times 10^{-5}$)	M_n ($\times 10^{-4}$)	Source
Poly(methyl methacrylate)	PMMA	1.05	4.82	Rohm and Haas
Poly(vinylidene fluoride)	PVDF	1.46	6.30	Pennwalt
Poly(styrene-*co*-acrylonitrile)	PSAN[a]	1.50	7.20	Dow Chemical

[a] Copolymer contains 25.3 wt% acrylonitrile

the manufacturer. Each grade of PMMA was melt-blended, using a twin-screw compounding machine, with PSAN and PVDF yielding the (a) PMMA/PVDF and (b) PMMA/PSAN blend systems, respectively. For each blend system, four blend compositions, namely 20/80, 40/60, 60/40, and 80/20 (by weight) were prepared.

Rheological measurements

A cone-and-plate rheometer (Weissenberg Rheogoniometer, Model R16) was used to measure (1) the steady shear flow properties, namely, the shear viscosity (η), the shear stress (σ), and the first normal stress difference (N_1), as functions of the shear rate ($\dot{\gamma}$), and (2) the oscillatory shearing flow properties, namely the dynamic storage modulus (G') and the dynamic loss modulus (G'') as functions of the angular frequency (ω). Rheological measurements were made at various temperatures, in order to investigate the temperature dependence of the rheological properties. So as to ensure that the measured viscoelastic properties would be in the linear region, a strain sweep was first made. Based on this measurement, a strain of ~ 0.005 was used for all of the measurements of G' and G''.

RESULTS

Figure 1 gives plots of $\log \eta$ and $\log N_1$ *versus* $\log \dot{\gamma}$, plus plots of $\log \eta'$ and $\log G'$ *versus* $\log \omega$, at three different temperatures for PMMA. It can be seen from the figure that at low values of $\dot{\gamma}$ and ω, η' is very close to η, while the values of G' are about one half of the value of N_1. *Figure 2* gives plots of $\log \eta_b$ *versus* $\log \dot{\gamma}$, and $\log \eta'_b$ *versus* $\log \omega$, for the PMMA/PSAN blend system at 200°C, while similar plots for the PMMA/PVDF blend system at 200°C are given in *Figure 3*. It can be seen in *Figures 2* and *3* that values of η_b and η'_b for the blend system lie between those of the constituent components. However, when we plot $\log \eta_b$ *versus* the blend composition using the data given in *Figure 3*, we obtain plots for the PMMA/PSAN blend system having *positive* deviations from the linear relationship and plots for the PMMA/PVDF blend system having *negative* deviations from the linear relationship. These observations will be discussed in greater detail below.

Figure 4 gives plots of $\log G'_b$ *versus* $\log G''_b$ for the PMMA/PVDF blend system at 210°C. For the sake of clarity, we chose not to include in *Figure 4* data points which were obtained at other temperatures. It should be noted that such plots are virtually independent of temperature[35–39]. It can be seen in *Figure 4* that plots of $\log G'_b$ *versus* $\log G''_b$ for all of the blend compositions lie between those of the constituent components, PMMA and PVDF, and that the melt elasticity of the PMMA/PVDF blends decreases monotonically with increasing amounts of the less-elastic component, PMMA.

Recently, Han[37] reported that for binary blends consisting of nearly monodisperse homopolymers with *identical* chemical structures, the $\log G'_b$ *versus* $\log G''_b$ plots at certain blend compositions lie above those obtained for the constituent components. However, as the polydispersity of the constituent components increases, thus leading to a considerable overlapping of

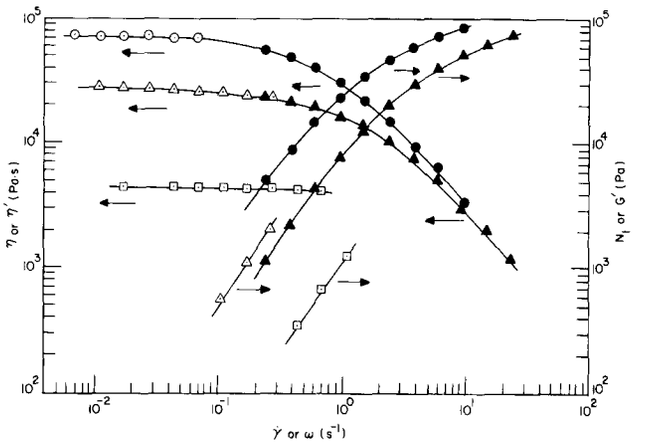

Figure 1 Plots of $\log \eta$ and $\log N_1$ *versus* $\log \dot{\gamma}$ (open symbols), and plots of $\log \eta'$ and $\log G'$ *versus* $\log \omega$ (filled symbols), for PMMA at different temperatures: (○, ●) 200; (△, ▲) 210; and (□, ■) 230°C

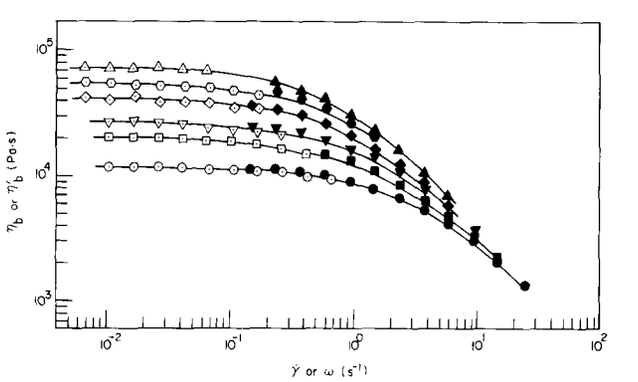

Figure 2 Plots of $\log \eta_b$ *versus* $\log \dot{\gamma}$ (open symbols), and plots of $\log \eta'_b$ *versus* $\log \omega$ (filled symbols), for the PMMA/PSAN blend system at 200°C: (△, ▲) PMMA; (○, ●) PSAN; (⊙, ●) 80/20 PMMA/PSAN blend; (◇, ◆) 60/40 PMMA/PSAN blend; (▽, ▼) 40/60 PMMA/PSAN blend; and (□, ■) 20/80 PMMA/PSAN blend

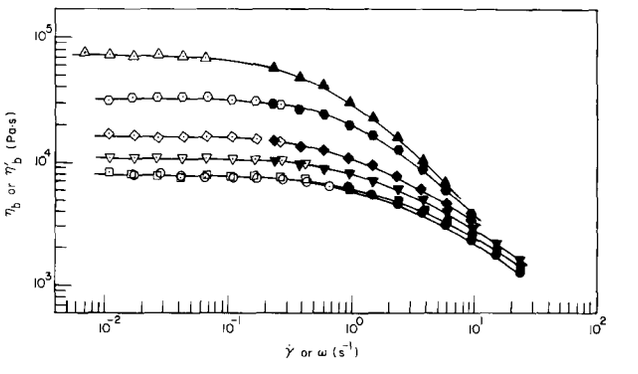

Figure 3 Plots of $\log \eta_b$ *versus* $\log \dot{\gamma}$ (open symbols), and plots of $\log \eta'_b$ *versus* $\log \omega$ (filled symbols), for the PMMA/PVDF blend system at 200°C: (△, ▲) PMMA; (○, ●) PVDF; (⊙, ●) 80/20 PMMA/PVDF blend; (◇, ◆) 60/40 PMMA/PVDF blend; (▽, ▼) 40/60 PMMA/PVDF blend; and (□, ■) 20/80 PMMA/PVDF blend

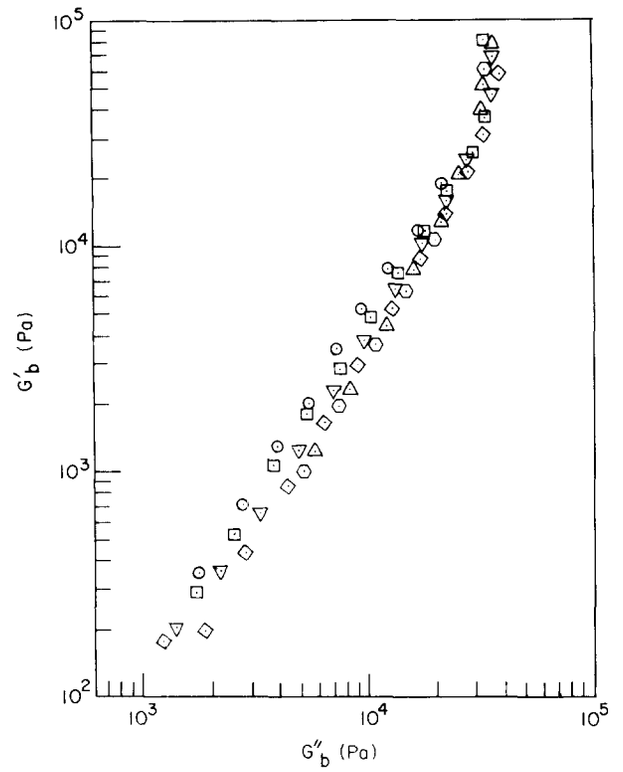

Figure 4 Plots of $\log G'_b$ *versus* $\log G''_b$ for the PMMA/PVDF blend system at 210°C: (△) PMMA; (○) PVDF; (⊙) 80/20 PMMA/PVDF blend; (◇) 60/40 PMMA/PVDF blend; (▽) 40/60 PMMA/PVDF blend; and (□) 20/80 PMMA/PVDF blend

molecular weight values between the two, the dependence of the $\log G'_b$ *versus* $\log G''_b$ plot on the blend composition is suppressed. This observation is relevant to the interpretation of the results given in *Figure 4*, because when dealing with binary blends consisting of components having *dissimilar* chemical structures, one usually finds two distinct curves in the $\log G'_b$ *versus* $\log G''_b$ plot, i.e. one for each constituent component. The extent of the spread of the two curves in the $\log G'_b$ *versus* $\log G''_b$ plots for a given polymer pair would depend on, among other factors, the extent of miscibility, polydispersities and plateau moduli of the constituent components. Therefore, the plots of $\log G'_b$ *versus* $\log G''_b$ for binary blends consisting of components having *dissimilar* chemical structures lie between those of the constituent components. However, it is possible that for certain polymer pairs consisting of monodisperse components with dissimilar chemical structures, the plots of $\log G'_b$ *versus* $\log G''_b$ at certain blend compositions may lie above those of the constituent components.

Let us now examine the dependence of the melt elasticity on the blend composition for binary blends of PMMA and PVDF under steady shear flow conditions. For this, plots of $\log N_{1b}$ *versus* $\log \sigma_b$ are given in *Figure 5* for the PMMA/PVDF blend system. Previous studies[38–41] show that plots of $\log N_1$ *versus* $\log \sigma$ for homopolymers are *virtually* independent of temperature. We conclude from *Figure 5* that the melt elasticity of PMMA/PVDF blends decreases monotonically with increasing amounts of the less-elastic component, PMMA. This conclusion is consistent with that made above using the plots of $\log G'_b$ *versus* $\log G''_b$ (see *Figure 4*).

Figure 6 gives plots of $\log G'_b$ *versus* $\log G''_b$ for the PMMA/PSAN blend system at 210°C. It can be seen in this figure that some of the plots obtained for certain blend compositions are not distinguishable from those of the pure PSAN component, and that the general spread of the plots for PSAN and PMMA is much smaller than that obtained for PVDF and PMMA (see *Figure 4*).

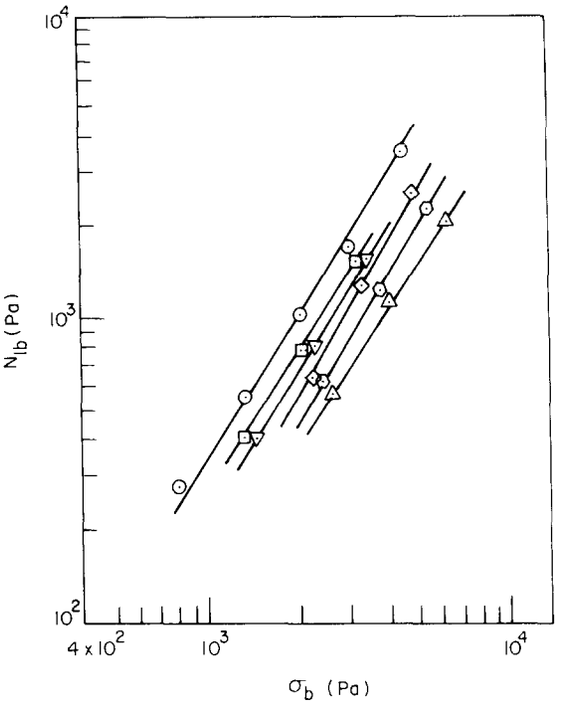

Figure 5 Plots of $\log N_{1b}$ *versus* $\log \sigma_b$ for the PMMA/PVDF blend system at 210°C: (△) PMMA; (○) PVDF; (⊙) 80/20 PMMA/PVDF blend; (◇) 60/40 PMMA/PVDF blend; (▽) 40/60 PMMA/PVDF blend; and (□) 20/80 PMMA/PVDF blend

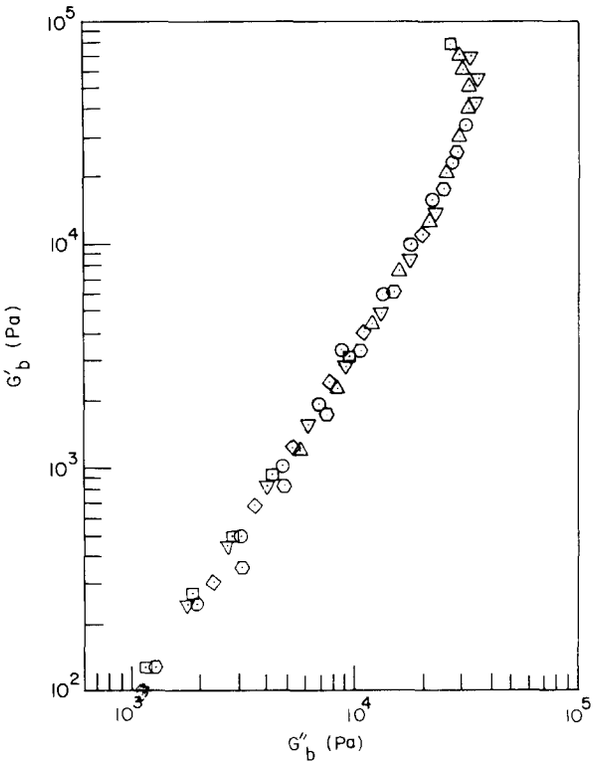

Figure 6 Plots of $\log G'_b$ *versus* $\log G''_b$ for the PMMA/PSAN blend system at 210°C: (△) PMMA; (○) PSAN; (⊙) 80/20 PMMA/PSAN blend; (◇) 60/40 PMMA/PSAN blend; (▽) 40/60 PMMA/PSAN blend; and (□) 20/80 PMMA/PSAN blend

THEORY

In dealing with the viscoelastic properties of two polydisperse polymers, which are relevant to the PMMA/PVDF and PMMA/PSAN blend systems used in our experimental study, Han and Kim[21] assumed that the relaxation modulus $G_b(t)$ of the blend is given by

$$G_b(t)=\sum_{i=1}^{n}\left\{\sum_{j=1}^{m}\left[G^o_{N_1}\frac{\phi_1}{m}w_{1i}F_{1i}(t)R_{1i}(t)+G^o_{N_2}\frac{\phi_2}{n}w_{2j}F_{2j}(t)R_{2j}(t)\right]\right\} \quad (1)$$

where the upper limit n (or m) in the summation notation denotes the number of fractions, chosen for computational purposes, in the constituent component 1 (or 2), with each having the molecular weight M_{1i} (or M_{2j}) and weight fraction w_{1i} (or w_{2j}), and ϕ_1 and ϕ_2 are the volume fractions of the constituent components. It should be noted that F_{kl} and R_{kl} in equation (1) are given by the following[21]:

$$F_{kl}(t)=\frac{4}{\pi^2}\sum_{p=1}^{\infty}\frac{H_{kl,p}}{p^2}\exp(-p^2t/\tau_{kl,p}) \quad (2)$$

$$R_{kl}(t)=\frac{1}{Z_{kl}}\sum_{s=1}^{Z_{kl}}\exp(-\lambda_{s,kl}t/2\tau_w) \quad (3)$$

$$(k=1,\ l=1,2,\ldots,n)$$

$$(k=2,\ l=1,2,\ldots,m)$$

where $\tau_{kl,p}$, $H_{kl,p}$, and $\lambda_{s,kl}$ (with $k=1,2$ in all three cases) are defined by:

$$\tau_{kl,p}=\tau_{d,kl}\Big/\left[1+\left(\frac{(-\chi)\phi^*_{kl}Z_{kl}}{p\pi}\right)^2\right]^2 \quad (4)$$

$$H_{kl,p}=\frac{1-(-1)^p\cosh[(-\chi)\phi^*_{kl}Z_{kl}]}{\{1+[(-\chi)\phi^*_{kl}Z_{kl}/p\pi]^2\}^2} \quad (5)$$

and

$$\lambda_{s,kl}=4\sin^2[\pi s/2(Z_{kl}+1)] \quad (6)$$

ϕ^*_{kl} is given by

$$\phi^*_{1l}=\frac{\phi_2 w_{2j}}{\rho_2}\Big/\left[\frac{\phi_1 w_{1i}}{\rho_1}+\frac{\phi_2 w_{2j}}{\rho_2}\right] \quad (7)$$

$$\phi^*_{2l}=1-\phi^*_{1l} \quad (8)$$

where ρ_i is the density of component i. τ_w in equation (3) is given by[42]:

$$\tau_w=\int_0^{\infty}\left[\phi_1\sum_{i=1}^{n}w_{1i}F_{1i}(t)+\phi_2\sum_{j=1}^{m}w_{2j}F_{2j}(t)\right]^z dt \quad (9)$$

z is a constraint release parameter which governs the strength of the constraint release contribution. It should be noted that for $z=3$, τ_w is given by equation (37) of ref. 21.

Using the expression for $G_b(t)$ given by equation (1), we can calculate the values of η_{ob}, $G'_b(\omega)$, and $G''_b(\omega)$ from

$$\eta_{ob}=\frac{4}{\pi^2}\sum_{i=1}^{n}\sum_{j=1}^{m}\left\{G^o_{N_1}\frac{\phi_1}{m}w_{1i}\left[\sum_{p=1}^{\infty}\frac{H_{1i,p}}{p^2}\frac{1}{Z_{1i}}\sum_{s=1}^{Z_{1i}}\tau_{1i,s}\right]+G^o_{N_2}\frac{\phi_2}{n}w_{2j}\left[\sum_{p=1}^{\infty}\frac{H_{2j,p}}{p^2}\frac{1}{Z_{2j}}\sum_{s=1}^{Z_{2j}}\tau_{2j,s}\right]\right\} \quad (10)$$

$$G'_b(\omega)=\frac{4}{\pi^2}\sum_{i=1}^{n}\sum_{j=1}^{m}\left\{G^o_{N_1}\frac{\phi_1}{m}w_{1i}\times\left[\sum_{p=1}^{\infty}\frac{H_{1i,p}}{p^2}\frac{1}{Z_{1i}}\sum_{s=1}^{Z_{1i}}\frac{(\omega\tau_{1i,s})^2}{1+(\omega\tau_{1i,s})^2}\right]+G^o_{N_2}\frac{\phi_2}{n}\times w_{2j}\left[\sum_{p=1}^{\infty}\frac{H_{2j,p}}{p^2}\frac{1}{Z_{2j}}\sum_{s=1}^{Z_{2j}}\frac{(\omega\tau_{2j,s})^2}{1+(\omega\tau_{2j,s})^2}\right]\right\} \quad (11)$$

$$G''_b(\omega)=\frac{4}{\pi^2}\sum_{i=1}^{n}\sum_{j=1}^{m}\left\{G^o_{N_1}\frac{\phi_1}{m}w_{1i}\times\left[\sum_{p=1}^{\infty}\frac{H_{1i,p}}{p^2}\frac{1}{Z_{1i}}\sum_{s=1}^{Z_{1i}}\frac{\omega\tau_{1i,s}}{1+(\omega\tau_{1i,s})^2}\right]+G^o_{N_2}\frac{\phi_2}{n}\times w_{2j}\left[\sum_{p=1}^{\infty}\frac{H_{2j,p}}{p^2}\frac{1}{Z_{2j}}\sum_{s=1}^{Z_{2j}}\frac{\omega\tau_{2j,s}}{1+(\omega\tau_{2j,s})^2}\right]\right\} \quad (12)$$

where

$$\frac{1}{\tau_{ki,s}}=\frac{p^2}{\tau_{ki,p}}+\frac{\lambda_{s,ki}}{2\tau_w} \qquad (k=1,2) \quad (13)$$

In order to minimize the computational time required for calculating the values of τ_w, which is defined by equation (37) in ref. 21, we use the following approximation:

$$\tau_w(\chi;\text{poly})=\tau_w(\chi;\text{mono})\left(\frac{\tau_w(\chi=0;\text{poly})}{\tau_w(\chi=0;\text{mono})}\right) \quad (14)$$

where 'poly' and 'mono' denote polydisperse and monodisperse components, respectively.

It should be noted that $\tau_w(\chi=0;\text{poly})$ in equation (14) for $z=3$ can be obtained from equation (41) of ref. 21:

$$\tau_w(\chi=0;\text{poly})=\left(\frac{8}{\pi^2}\right)^3\sum_{i=1}^{2}\sum_{j=1}^{2}\sum_{k=1}^{2}\phi_i\phi_j\phi_k\left\{\sum_{l=1}^{N'}\sum_{u=1}^{N''}\sum_{v=1}^{N'''}\times w_{il}w_{ju}w_{kv}\left[\sum_{\substack{p=1\\ \text{odd}}}^{\infty}\sum_{\substack{q=1\\ \text{odd}}}^{\infty}\sum_{\substack{r=1\\ \text{odd}}}^{\infty}\frac{1}{p^2}\frac{1}{q^2}\frac{1}{r^2}\Big/\left(\frac{p^2}{\tau_{di,l}}+\frac{q^2}{\tau_{dj,u}}+\frac{r^2}{\tau_{dk,v}}\right)\right]\right\} \quad (15)$$

where

$$N'=\begin{cases}n & \text{for } i=1\\ m & \text{for } i=2\end{cases};\quad N''=\begin{cases}n & \text{for } j=1\\ m & \text{for } j=2\end{cases};$$

$$N'''=\begin{cases}n & \text{for } k=1\\ m & \text{for } k=2\end{cases} \quad (16)$$

and $\tau_{dk,i}$ in equation (15) is given by

$$\tau_{dk,i}(M_{k,i})=\tau_{dk}(M_{w,k})\left(\frac{M_{k,i}}{M_{w,k}}\right)^{3.4} \quad (17)$$

where

$$\tau_{dk}(M_{w,k})=\left(\frac{12}{\pi^2}\right)\frac{\eta_{o,k}}{G^o_{N,k}} \quad (18)$$

$$(k=1;\quad i=1,2,\ldots,n)$$

$$(k=2;\quad i=1,2,\ldots,m)$$

in which $M_{w,k}$ and η_{ok} are the weight-average molecular weight and zero-shear viscosity, respectively, of component k. Equation (17) implies that we used an empirical relationship, i.e. $\eta\sim\tau_d\sim M^{3.4}$, rather than the tube model[43] which predicts $\eta\sim M^3$.

In addition, $\tau_w(\chi=0;$ mono) in equation (14) for $z=3$ can easily be obtained from equation (15) by setting $N'=N''=N'''=1$ and $w_{il}=w_{ju}=w_{kv}=1$. Finally, $\tau_w(\chi=0;$ mono) in equation (14) for $z=3$ can be obtained from equation (12) of ref. 21:

$$\tau_w=\left(\frac{4}{\pi^2}\right)^3\left\{\sum_{i=1}^{2}\sum_{j=1}^{2}\sum_{k=1}^{2}\phi_i\phi_j\phi_k\sum_{p}^{\infty}\sum_{q}^{\infty}\sum_{r}^{\infty}\times\left(\frac{H_{i,p}}{p^2}\right)\left(\frac{H_{j,q}}{q^2}\right)\left(\frac{H_{k,r}}{r^2}\right)\Bigg/\left(\frac{p^2Q_{i,p}}{\tau_{di}}+\frac{q^2Q_{j,q}}{\tau_{dj}}+\frac{r^2Q_{k,r}}{\tau_{dk}}\right)\right\} \quad (19)$$

COMPARISON OF THEORY WITH EXPERIMENT

In order to offer a theoretical interpretation of the experimental results presented above, we calculated, using equations (10)–(12), values of η_{ob}, G'_b, and G''_b by dividing each component into seven fractions (i.e. $n=m=7$), for which the log-normal distribution function was assumed to represent the molecular weight distribution of the pure components. It should be borne in mind that the PMMA, PVDF and PSAN materials employed in this study are polydisperse (see *Table 1*). We were well aware of the fact that the larger the number of fractions for each component, the more accurate the predicted values. However, we found that the computational time increased very rapidly with increase in the number of fractions for each component and thus we had to balance the accuracy of prediction against the computational time that was required.

In the computations, we used the following numerical values for the plateau modulus G_N^0: 6.0×10^5 Pa for PMMA, 4.0×10^5 PA for PVDF, and 2.28×10^5 Pa for PSAN[44]. We also used (i) $z=3$ for both PMMA/PSAN and PMMA/PVDF blend systems, (ii) $\chi=-0.3$ for PMMA/PVDF blends[29,33], and (iii) $\chi=-0.01$ for PMMA/PSAN blends[45]. It should be noted that z may be regarded as an adjustable parameter[42]. However, in this present study we chose not to vary the value of z. It has been reported in the literature[46,47] that the value of z varies from 3 to 20, depending on the blend system that is being studied.

We found that the predicted values of η_o for the polydisperse and pure components, when using equations (10) and (14)–(19), did not agree with the experimental results. Therefore, in order to match the predicted values of η_{ob} with the measured ones we employed the following procedures. First, the values of η_{ob} were calculated using equation (10) with the aid of equation (17) and secondly, the calculated values of η_{ob} were compared with the experimental results. Where there was discrepancy between the two, an iterative procedure was employed to improve the values of $\tau_{dk}(M_{w,k})$ using

$$\tau_{dk}^{(j+1)}(M_{w,k})=\tau_{dk}^{(j)}(M_{w,k})\left(\frac{\eta_{ok}}{\eta_{ok,c}^{(j)}}\right) \quad (20)$$

where $\eta_{ok,c}^{(j)}$ is the calculated value of the zero-shear viscosity at the jth iteration. In the final stage the first two steps were repeated until convergence was obtained with the tolerance, $|\eta_{ok,c}-\eta_{ok}|/\eta_{ok}\leqslant10^{-7}$.

Using the values of $\tau_{dk}(M_{w,k})$ $(k=1,2)$ that were calculated with the procedures described above, we predicted the values of η_{ob}, $G'_b(\omega)$, and $G''_b(\omega)$ for the PMMA/PVDF and PMMA/PSAN blends, where each consisted of polydisperse constituent components. *Figure 7* gives plots of log $G'_b(\omega)$ *versus* log ω, and *Figure 8* gives

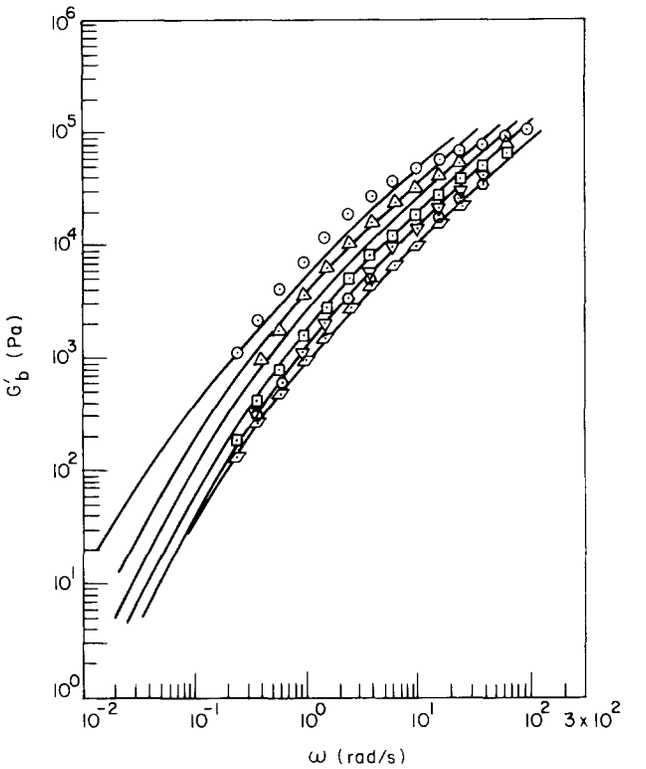

Figure 7 Comparison of predicted (continuous curves) with experimentally determined log G'_b *versus* log ω plots for the PMMA/PVDF blend system at 210°C: (⊙) PMMA; (⊙) PVDF; (△) 80/20 PMMA/PVDF blend; (⊡) 60/40 PMMA/PVDF blend; (▽) 40/60 PMMA/PVDF blend; and (◇) 20/80 PMMA/PVDF blend. $\chi=-0.3$ and $z=3$ were used in the calculations of the predicted curves

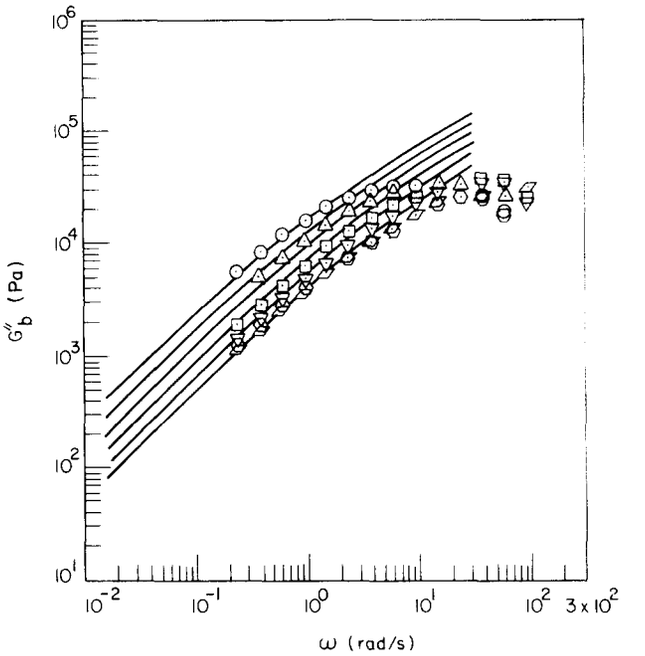

Figure 8 Comparison of predicted (continuous curves) with experimentally determined log G''_b *versus* log ω plots for the PMMA/PVDF blend system at 210°C: (⊙) PMMA; (⊙) PVDF; (△) 80/20 PMMA/PVDF blend; (⊡) 60/40 PMMA/PVDF blend; (▽) 40/60 PMMA/PVDF blend; and (◇) 20/80 PMMA/PVDF blend. $\chi=-0.3$ and $z=3$ were used in the calculations of the predicted curves

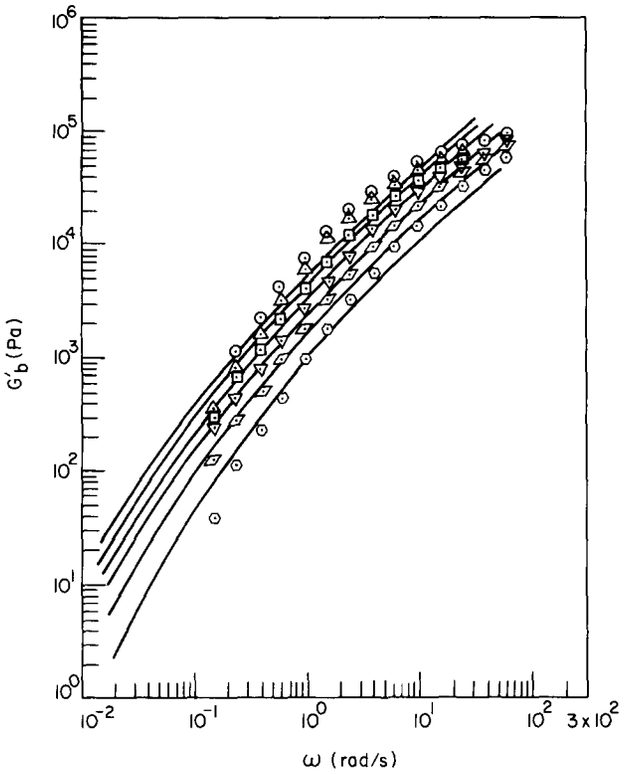

Figure 9 Comparison of predicted (continuous curves) with experimentally determined log G'_b *versus* log ω plots for the PMMA/PSAN blend system at 210°C: (⊙) PMMA; (⊙) PSAN; (△) 80/20 PMMA/PSAN blend; (⊡) 60/40 PMMA/PSAN blend; (▽) 40/60 PMMA/PSAN blend; and (◇) 20/80 PMMA/PSAN blend. $\chi = -0.01$ and $z = 3$ were used in the calculations of the predicted curves

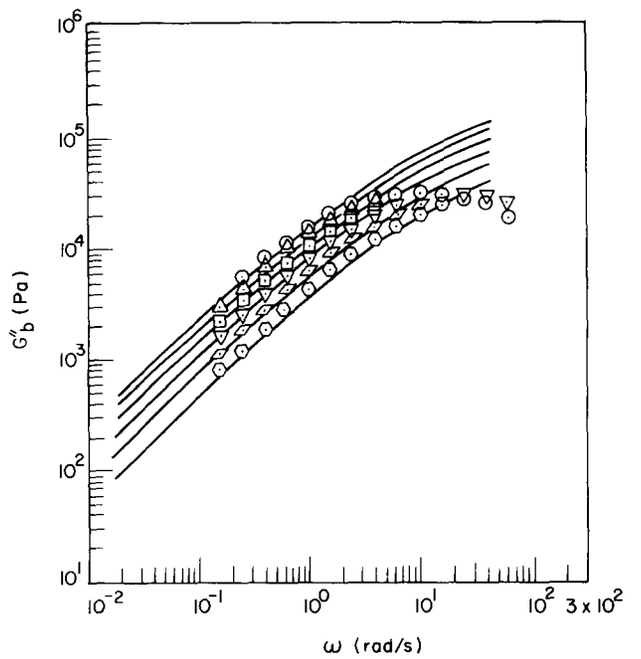

Figure 10 Comparison of predicted (continuous curves) with experimentally determined log G''_b *versus* log ω plots for the PMMA/PSAN blend system at 210°C: (⊙) PMMA; (⊙) PVDF; (△) 80/20 PMMA/PVDF blend; (⊡) 60/40 PMMA/PVDF blend; (▽) 40/60 PMMA/PVDF blend; and (◇) 20/80 PMMA/PVDF blend. $\chi = -0.01$ and $z = 3$ were used in the calculations of the predicted curves

plots of log $G''_b(\omega)$ *versus* log ω, for the PMMA/PVDF blends at 210°C, in which the continuous curves represent the predictions. Similar plots are given in *Figures 9* and *10* for the PMMA/PSAN blends at 210°C. It can be seen from *Figures 7–10* that the predictions are in good agreement with the experimental results at small values of ω (i.e. in the terminal region), but they deviate appreciably from the experimental results at large values of ω.

Recently, in investigating the effect of polydispersity on the linear viscoelastic properties of entangled homopolymers, Wasserman and Graessley[48] used a quadratic blending law[49] for the stress relaxation modulus $G_b(t)$:

$$G_b(t) = G_N^0 \left\{ \sum_{i=1}^{\infty} w_i [F_i(t)]^{1/2} \right\}^2 \tag{21}$$

where

$$F_i(t) = \frac{8}{\pi^2} \sum_{\substack{p \\ \text{odd}}}^{\infty} \frac{1}{p^2} \exp(-p^2 t/\tau_{di}) \tag{22}$$

in which τ_{di} is the tube disengagement time for fraction i. In doing so, Wasserman and Graessley modified $F_i(t)$ using the approach of des Cloizeaux[50], which neglects the contribution of constraint release, and calculated the values of $G'(\omega)$ and $G''(\omega)$, which agreed reasonably well with the experimental results, for a polydisperse homopolymer. It should be mentioned that due to the non-linear nature of equation (21), a numerical method must be used to calculate the values of η_o, $G'(\omega)$ and $G''(\omega)$, while in the present study we used analytical expressions, i.e. equations (10)–(12).

Figure 11 gives a comparison of prediction with

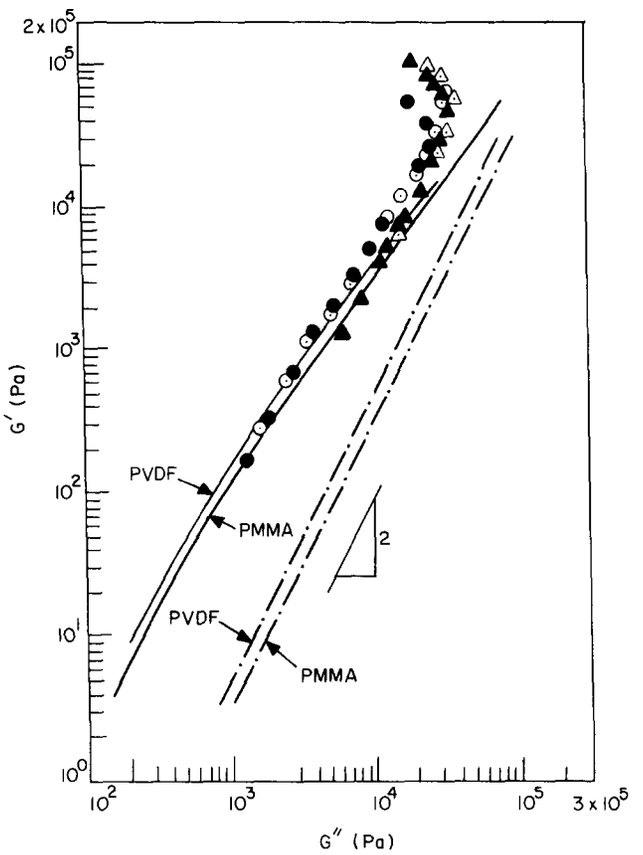

Figure 11 Comparison of predicted with experimentally determined log G'_b *versus* log G''_b plots for PMMA and PVDF: (△) data for PMMA at 200°C; (▲) data for PMMA at 210°C; (⊙) data for PVDF at 200°C; and (●) data for PVDF at 210°C. Continuous curves represent the predicted values for the polydisperse components, while the broken curves represent the predicted values for the monodisperse components; $\chi = -0.3$ and $z = 3$ were used in the calculations of the predicted curves

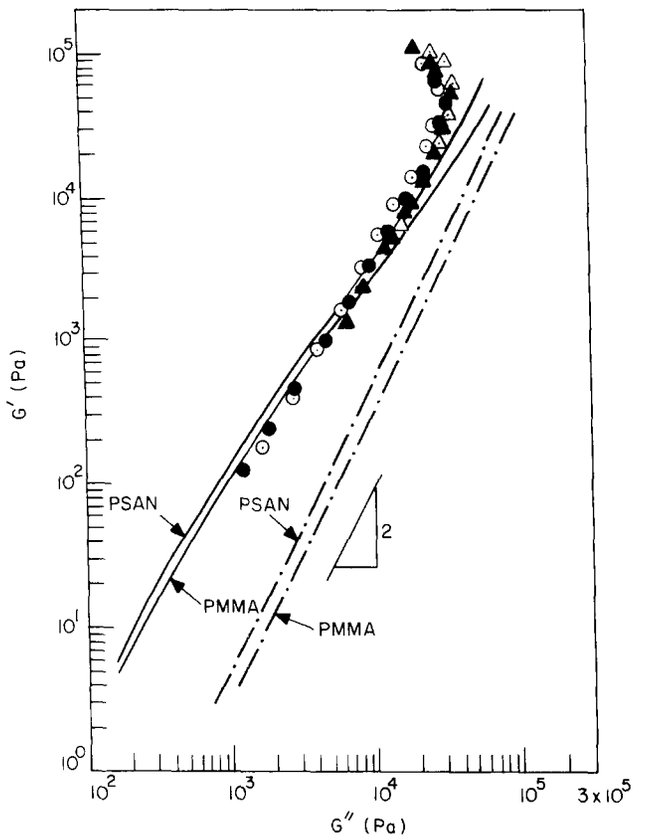

Figure 12 Comparison of predicted with experimentally determined log G'_b *versus* log G''_b plots for PMMA and PSAN: (△) data for PMMA at 200°C; (▲) data for PMMA at 210°C; (⊙) data for PSAN at 200°C; and (●) data for PSAN at 210°C. Continuous curves represent the predicted values for the polydisperse components, while the broken curves represent the predicted values for the monodisperse components; $\chi = -0.01$ and $z = 3$ were used in the calculations of the predicted curves

experiment for plots of log G' *versus* log G'' for PMMA and PVDF. Similar plots are given in *Figure 12* for PMMA and PSAN. For clarity, neither the experimental data nor the predictions for the blends are given in *Figures 11* and *12* because we have found that they lie between the values of the constituent components. According to Han and coworkers[6,7,17,18], the effect of blend composition on the melt elasticity in polymer blends can best be examined by using plots of log G'_b *versus* log G''_b. The following observations are worth noting concerning the theoretical predictions given in *Figures 11* and *12*.

(1) Plots of log G' *versus* log G'' for the polydisperse PVDF lie slightly above those for the polydisperse PMMA, whereas plots of log G' *versus* log G'' for the monodisperse PVDF lie significantly above those of the monodisperse PMMA. In other words, the polydispersity of PMMA and PVDF smears out the difference existing in the melt elasticity between the two components. We can now understand why the experimentally determined plots of log G'_b *versus* log G''_b for various blend compositions in the PMMA/PVDF blend system (see *Figure 4*) and in the PMMA/PSAN blend system (see *Figure 6*) lie very close to each other.

(2) Plots of log G' *versus* log G'' for the polydisperse components lie above those of the monodisperse components, as shown previously[21].

A comparison of the predictions of the composition-dependent η_{ob} with the experimental results is given in *Figure 13* for PMMA/PSAN blends, and in *Figure 14* for PMMA/PVDF blends, at temperatures of 200 and 210°C. It can be seen in *Figure 13* that agreement between prediction and experiment is very good for the PMMA/PSAN blends, in which the value of $\chi = -0.01$ was used in the prediction. We find, however, (see *Figure 14*) that the extent of agreement between theory and experiment for PMMA/PVDF blends depends on the value of χ, i.e. the use of $\chi = -0.5$ gives a better agreement with experiment than the use of $\chi = -0.3$. It should be mentioned that in obtaining the predictions given in *Figure 14* we used a single value of χ for all blend compositions. There is, however, experimental evidence to suggest that the value of χ for the PMMA/PVDF blend system may vary with blend composition[33].

For blends, such as the PMMA/PVDF blend system, exhibiting a lower critical solution temperature (*LCST*) behaviour, the value of $-\chi$ will increase with decreasing temperature. In view of the fact that theoretical predictions of η_{ob} are very sensitive to χ, the discrepancies in η_{ob} between the predictions and the experimental results, observed in *Figure 14*, may be attributable, at least in part, to the use of constant values of χ in the predictions. We conclude, therefore, that there is an urgent need for an accurate determination of χ for miscible polymer blends, especially for those blends that have strong interactions between the constituent components.

As discussed elsewhere[21], the Han–Kim theory gives only a poor prediction of the composition dependence of zero-shear viscosity for the PMMA/PVDF blend system, even if we include a polydispersity effect. For the PMMA/PVDF blends, we found that there are large differences in the temperature dependence of viscosity between PMMA and PVDF (see *Figure 15*). It should be noted that for the PMMA/PSAN blends, there is little

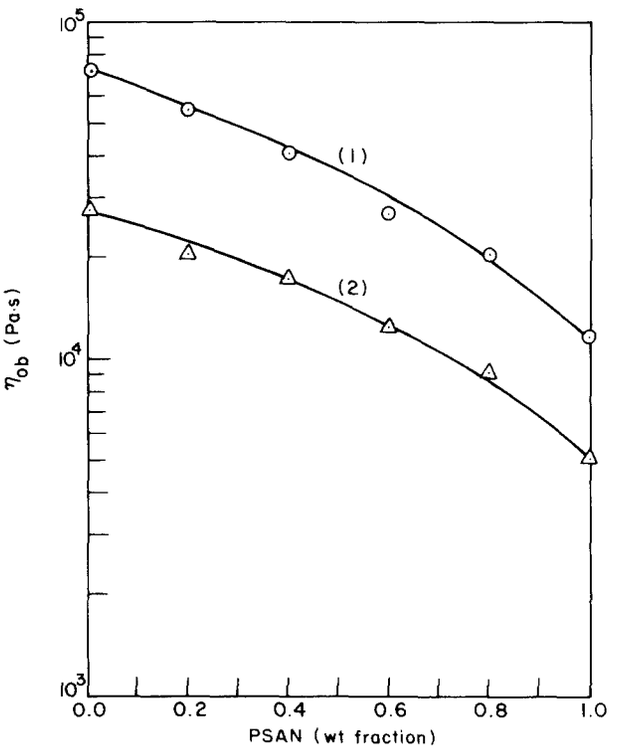

Figure 13 Comparison of predicted (continuous curves) with experimentally determined log η_{ob} *versus* blend composition plots for the PMMA/PSAN blend system: (⊙) data at 200°C and (△) data at 210°C. Curve 1 represents the predicted values at 200°C while curve 2 represents the predicted values at 210°C; $\chi = -0.01$ and $z = 3$ were used in the calculations of the predicted curves

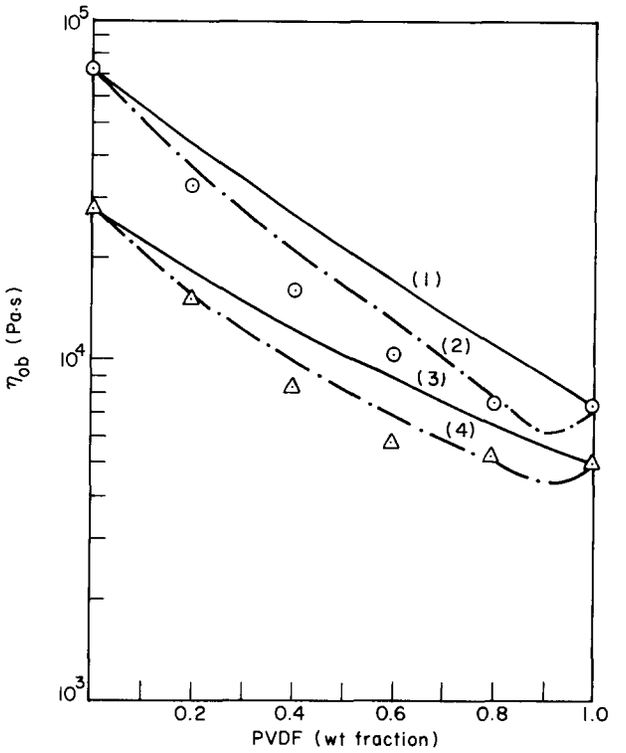

Figure 14 Comparison of predicted with experimentally determined log η_{ob} *versus* blend composition plots for the PMMA/PVDF blend system: (⊙) data at 200°C and (△) data at 210°C. Continuous curve 1 represents the predicted values at 200°C, with $\chi = -0.3$ and $z = 3$; broken curve 2 represents the predicted values at 200°C, with $\chi = -0.5$ and $z = 3$; continuous curve 3 represents the predicted values at 210°C, with $\chi = -0.3$ and $z = 3$; broken curve 4 represents the predicted values at 210°C, with $\chi = -0.5$ and $z = 3$

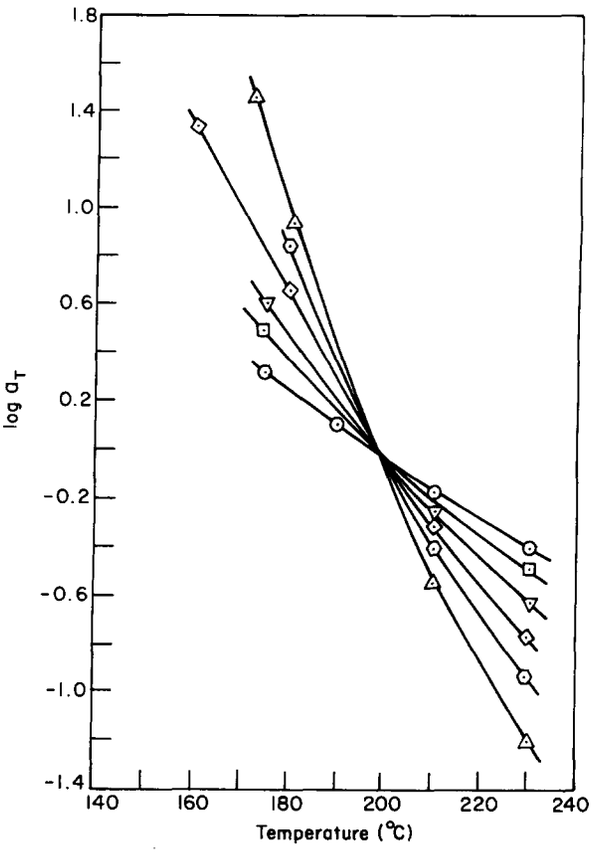

Figure 15 Plots of log a_T *versus* temperature for the PMMA/PVDF blend system using a reference temperature of 190°C: (△) PMMA; (⊙) PVDF; (⊙) 80/20 PMMA/PVDF blend; (◇) 60/40 PMMA/PVDF blend; (▽) 40/60 PMMA/PVDF; and (□) 20/80 PMMA/PVDF blend

difference in the values of the shift factor a_T between PMMA and PSAN (as shown in *Figure 16*).

It has been suggested[3,14,16] that the effect of blend composition on the viscosity of miscible polymer blends, which consist of two *amorphous* polymers, should be investigated under iso-free-volume conditions, or at temperatures which are at an equal distance from the T_gs of the respective blend compositions. Specifically, Aoki[16] reported that for miscible blends of poly[styrene-*co*-(*N*-phenylmaleimide)] (PSPM) and PSAN, plots of log η_{ob} *versus* blend composition exhibited negative deviations from linearity under isothermal conditions, but positive deviations from linearity under iso-free-volume conditions. Aoki[16] demonstrated for the PSPM/PSAN blend system that plots of log a_T *versus* temperature became independent of blend composition when the T_g of each blend composition was used as the reference temperature, whereas plots of log a_T *versus* temperature varied with blend composition when 200°C was used as the reference temperature for all blend compositions. The concept of the iso-free volume is very useful for blend systems where the constituent components are amorphous and particularly when the temperature dependence of log a_T on blend composition is very small, which is the case for the PMMA/PSAN blends. However, when one of the constituent components in a miscible blend is crystalline, as is the case for PMMA/PVDF blends, the use of the iso-free volume conditions is not straightforward. In such a situation, we believe that the melting point of a crystalline component plays a more important role than the glass transition temperature in determining the viscoelastic properties of miscible polymer blends in the

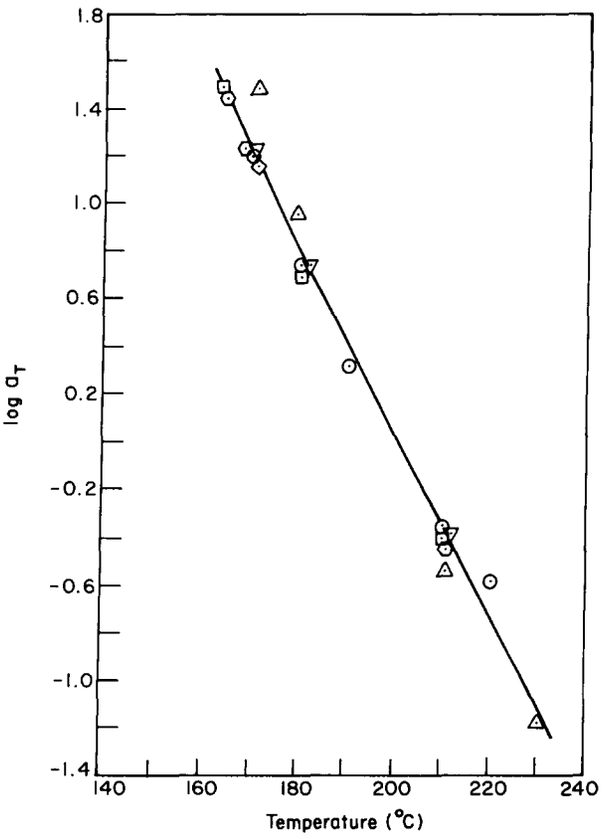

Figure 16 Plots of log a_T *versus* temperature for the PMMA/PSAN blend system using a reference temperature of 190°C: (△) PMMA; (⊙) PSAN; (⊙) 80/20 PMMA/PSAN blend; (◇) 60/40 PMMA/PSAN blend; (▽) 40/60 PMMA/PSAN blend; and (□) 20/80 PMMA/PSAN blend

molten state. For a blend where the dependence of log a_T on blend composition is very large, which is the case for PMMA/PVDF blends, the relative temperature dependence of the dynamics may play a greater role than the thermodynamics of mixing, the topology of the blend system, or the polydispersity effect.

CONCLUSIONS

In this study we have shown experimentally that plots of $\log \eta_{ob}$ *versus* blend composition at a constant temperature show negative deviations from linearity for the miscible PMMA/PVDF blend system, but positive deviations from linearity for the miscible PMMA/PSAN system. We have explained the experimental results using the molecular viscoelasticity theory of Han and Kim[20,21]. Specifically, according to this theory, the negative deviation observed in the plots of η_{ob} *versus* blend composition for the PMMA/PVDF blend system is attributed to a sufficiently large value of the interaction parameter $|\chi|$ for the PMMA/PVDF pair, and the positive deviation observed in the plot of $\log \eta_{ob}$ *versus* blend composition for the PMMA/PSAN blend system is attributed to the very small value of $|\chi|$ for the PMMA/PSAN pair.

As described in ref. 20, the good agreement between theory and experiment observed above does not necessarily warrant the use of the position-independent potential function. Rigorously speaking, the potential function must be obtained by using a self-consistent method and it may turn out to be position-dependent.

In this present study we used a linear blending law for the stress relaxation modulus, given by equation (1). Recently, Composto *et al.*[51] used a similar expression to investigate mutual diffusion in a blend of polystyrene and poly(2,6-dimethyl-1,4-phenylene ether). They reported that the friction coefficient of the blend could not be described by a weighted average of the friction coefficients of the constituent components[52]. More recently, Zawada *et al.*[53] also reported similar results for blends of PMMA and poly(ethylene oxide). On the basis of these studies we are of the opinion that the constraint release mechanism between two chains having dissimilar chemical structures may not be the same as that between two chains which have an identical chemical structure.

Finally, in order to critically test a molecular theory predicting the rheological properties of miscible polymer blends, it is very important to select a miscible pair of polymers which have the following features: (a) the T_gs of the constituent components are not too far apart, giving rise to a iso-free-volume state; (b) the molecular-weight distribution of the constituent components is as narrow as possible, making the polydispersity effect insignificant; (c) both constituent components are amorphous; and (d) the dependencies of the interaction parameter on both blend composition and temperature are known.

REFERENCES

1 Olabisi, O., Robeson, L. M. and Shaw, M. T. 'Polymer–Polymer Miscibility', Academic, New York, 1979, Ch. 5, p. 215
2 Krause, S. in 'Polymer Blends' (Eds. D. R. Paul and S. Newman), Vol. 1, Academic, New York, 1977, Ch. 2, p. 15
3 Prest, W. M. and Porter, R. S. *J. Polym. Sci. (A-2)* 1972, **10**, 1639
4 Aoki, Y. *Polym. J.* 1984, **16**, 431
5 Wisniewsky, C., Marin, G. and Monge, P. *Eur. Polym. J.* 1984, **20**, 691
6 Chuang, H. K. and Han, C. D. *J. Appl. Polym. Sci.* 1984, **29**, 2205
7 Han, C. D. and Yang, H. H. *J. Appl. Polym. Sci.* 1987, **33**, 1199
8 Martuscelli, E., Vicini, L. and Sever, A. *Makromol. Chem.* 1987, **188**, 607
9 Wu, S. *J. Polym. Sci. Polym. Phys. Edn* 1987, **25**, 557
10 Wu, S. *Polymer* 1987, **28**, 1144
11 Wu, S. *J. Polym. Sci. Polym. Phys. Edn* 1987, **25**, 2511
12 Stadler, R., Freitas, L. L., Krieger, V. and Klotz, S. *Polymer* 1988, **29**, 1643
13 Ajii, A., Choplin, L. and Prud'homme, R. E. *J. Polym. Sci. Polym. Phys. Edn* 1988, **26**, 2279
14 Aurelio de Araujo, M. and Stadler, R. *Makromol. Chem.* 1988, **189**, 2169
15 Roland, C. M. *J. Polym. Sci. Polym. Phys. Edn* 1988, **26**, 839
16 Aoki, Y. *Macromolecules* 1990, **23**, 2309
17 Kim, J. K., Han, C. D. and Lee, Y. J. *Polym. J.* 1992, **24**, 205
18 Han, C. D., Chung, H. S. and Kim, J. K. *Polymer* 1992, **33**, 546
19 Roovers, J. and Toporowski, P. M. *Macromolecules* 1992, **25**, 1096
20 Han, C. D. and Kim, J. K. *Macromolecules* 1989, **22**, 1914
21 Han, C. D. and Kim, J. K. *Macromolecules* 1989, **22**, 4292
22 Stein, D. J., Jung, R. H., Illers, K. H. and Hendus, H. *Angew. Makromol. Chem.* 1974, **36**, 89
23 McMaster, L. P. in 'Copolymers, Polyblends, and Composites' (Ed. N. A. J. Platzer) ACS Advances in Chemistry Series, Vol. 142, American Chemical Society, Washington, DC, 1975, p. 43
24 Kruse, W. A., Kirste, R. G., Haas, J., Schmitt, B. J. and Stein, D. *J. Makromol. Chem.* 1976, **177**, 1145
25 Bernstein, R. E., Cruz, C. A., Paul, D. R. and Barlow, J. W. *Macromolecules* 1977, **10**, 681
26 Naito, K., Johnson, R. E., Allara, K. L. and Kwei, T. K. *Macromolecules* 1978, **11**, 1260
27 McBriety, V. J., Douglass, D. C. and Kwei, T. K. *Macromolecules* 1978, **11**, 1265
28 Noland, J. S., Hsu, H. C., Saxon, R. and Schmitt, J. M. in 'Multicomponent Polymer Systems' (Ed. N. A. J. Platzer), ACS Advances in Chemistry Series, Vol. 99, American Chemical Society, Washington, DC, 1971, p. 15
29 Nishi, T. and Wang, T. T. *Macromolecules* 1975, **8**, 909
30 Kwei, T. K., Frisch, H. L., Radigan, W. and Vogel, S. *Macromolecules* 1977, **10**, 157
31 Wang, T. T. and Nishi, T. *Macromolecules* 1977, **10**, 142
32 Paul, D. R. and Altamirano, J. O. in 'Copolymers, Polyblends and Composites', (Ed. N. A. J. Platzer), ACS Advances in Chemistry Series, Vol. 142, American Chemical Society, Washington, DC, 1975, p. 371
33 Wendorff, J. H. *J. Polym. Sci. Polym. Lett. Edn* 1980, **18**, 439
34 Ward, T. C. and Lin, T. S. in 'Polymer Blends and Composites in Multiphase Systems' (Ed. C. D. Han), ACS Advances in Chemistry Series, Vol. 206, American Chemical Society, Washington, DC, 1984, p. 59
35 Han, C. D. and Jhon, M. S. *J. Appl. Polym. Sci.* 1986, **32**, 3809
36 Han, C. D. and Lem, K. W. *Polym. Eng. Rev.* 1983, **2**, 135
37 Han, C. D. *J. Appl. Polym. Sci.* 1988, **35**, 167
38 Han, C. D. *Trans. Soc. Rheol.* 1974, **18**, 163
39 Han, C. D. 'Rheology in Polymer Processing', Academic, New York, 1976
40 Han, C. D. 'Multiphase Flow in Polymer Processing', Academic, New York, 1981
41 Oda, K., White, J. L. and Clark, E. S. *Polym. Eng. Sci.* 1978, **18**, 25
42 Graessley, W. W. *Adv. Polym. Sci.* 1982, **47**, 67
43 Doi, M. and Edwards, S. F. *J. Chem. Soc. Faraday Trans. 2* 1978, **74**, 1789, 1802
44 Yang, H. H. *PhD Thesis*, Brooklyn Polytechnic University, New York, NY, 1988
45 Schmitt, B. J., Kirste, R. G. and Jelenic, J. *Makromol. Chem.* 1980, **181**, 1655
46 Struglinski, M. J. *PhD Thesis*, Northwestern University, Evanston, IL, 1984
47 Composto, R. J. *PhD Thesis*, Cornell University, Ithaca, NY, 1987
48 Wasserman, S. H. and Graessley, W. W. *J. Rheol.* 1992, **36**, 543
49 Tsenoglou, C. *Macromolecules* 1991, **24**, 1762
50 des Cloizeaux, J. *Macromolecules* 1990, **23**, 4678
51 Composto, R. J., Kramer, E. J. and White, D. M. *Macromolecules* 1992, **25**, 4167
52 Composto, R. J., Kramer, E. J. and White, D. M. *Polymer* 1990, **31**, 2320
53 Zawada, J. A., Ylitalo, C. M., Fuller, G. G., Colby, R. H. and Long, T. E. *Macromolecules* 1992, **25**, 2896